

Breast lesion detection and visualization utilizing artificial intelligence and the H-scan

Jihye Baek
Department of Electrical and Computer
Engineering
University of Rochester
Rochester, NY, USA
jbaek7@ur.rochester.edu

Avice M. O'Connell
Department of Imaging Sciences
University of Rochester Medical Center
Rochester, NY, USA
avice_oconnell@URMC.Rochester.edu

Kevin J. Parker
Department of Electrical and Computer
Engineering
University of Rochester
Rochester, NY, USA
kevin.parker@rochester.edu

Abstract— We incorporated raw ultrasound parameters into artificial intelligence-based breast cancer diagnosis to achieve improved accuracy compared to radiologists and deep learning (DL).

76 patients with suspicious breast lesions were ultrasound-imaged using a Samsung RS85 system equipped with a 9.4 MHz center frequency transducer. The patients underwent biopsy, and the biopsy results were used as a reference gold standard: $n=53$ for benign and $n=23$ for malignant. Ten radiologists reviewed the ultrasound images and provided BI-RADS (Breast Imaging Reporting and Data System) scores.

A previously trained DL product with a modified fully convolutional network and GoogLeNet contoured the breast lesion boundaries. Within the contoured lesions, ultrasound parameters were extracted from the radiofrequency, envelope, and log-compressed data: (1) H-scan color level, (2) lesion boundary shape using convex hull, (3) B-mode boundary standard deviation (STD), (4) B-mode STD, and (5) Burr distribution b . To quantify breast condition, multiparametric analysis combining the 5 features was performed using principal component analysis, resulting in the first principal component (PC1). The PC1 outputs within a lesion were overlaid on B-mode images. We calculated the area under the curve (AUC) to evaluate performance.

We compared AUC results from radiologists, the DL product, and our PC1 quantification. The PC1 showed the highest AUC. Further, utilizing this PC1 quantification, we visualized the localized probability of malignancy, illustrating BI-RADS score differences using a color display. Overall, we demonstrated the potential of utilizing raw ultrasound parameters to improve DL performance and to achieve higher diagnostic accuracy than radiologists for breast cancer.

Keywords— *Biophysical ultrasound feature, Breast cancer diagnosis, Machine learning, Multiparametric analysis, Multiparametric imaging, Tissue characterization*

I. INTRODUCTION

There are a growing number of approaches that incorporate developments in artificial intelligence (AI) into the diagnosis of breast cancer using medical imaging [1-4]. Among AI applications to medical imaging, machine learning (ML) methods [5-8], such as support vector machine and random forest, were utilized to classify breast lesions as malignant or benign. ML requires feature extraction and selection procedures, which determines the classification accuracy. However, deep learning (DL) methods can directly utilize images as input, discarding feature dependency; DL can classify and segment breast lesions [9-15]. Due to the

image input processing, DL is computationally expensive, and thus it is common to use log-compressed envelope ultrasound data as input, which has less information than the raw ultrasound radiofrequency (RF) data. Utilizing the image data after RF information loss may lower DL performance.

This study aimed to develop a breast cancer detection method utilizing AI results and further adding ultrasound parameters, including frequency domain analysis, via H-scan. We employed the H-scan analysis since previous studies reported that the H-scan can successfully characterize tissue signatures, for example, differentiating liver diseases (inflammation, fibrosis, steatosis, and pancreatic cancer metastasis in liver) [16-20], distinguishing melanoma metastases [21], predicting thyroid malignancy [22], and detecting breast cancer response to treatment [23]. In this study, we segmented breast lesions using DL with log-compressed images and then added more information from features extracted from RF data. This approach resulted in higher diagnostic accuracy than both radiologists and a DL system.

II. METHODS

A. Study protocol

At the University of Rochester Medical Center, 76 patients with at least one suspicious breast lesion were enrolled in this study and underwent ultrasound scans. The breast lesions were examined by biopsy to diagnose the status as benign or malignant; the biopsy results were used as the gold standard.

The breast lesions were ultrasound-imaged using an RS85 ultrasound scanner (Samsung Medison Co. Ltd., South Korea) equipped with a 3–12 MHz linear array transducer (L3-12A), all with the following scanning conditions: (1) using a 9.4 MHz center frequency transmission; (2) without using harmonic mode. The ultrasound scanner saved RF data and post-processed log-compressed data, which were used for our data analysis.

The ultrasound breast images were reviewed by ten radiologists to provide the Breast Imaging Reporting and Database System (BI-RADS) scores. The ten scores for each patient were averaged using the area-preserving method of averaging receiver operating characteristic curves [24]. The BI-RADS score represents the performance of radiologists in breast lesion diagnosis.

This study was approved by the Research Subjects Review Board at the University of Rochester and performed under the requirements of informed consent.

B. Breast lesion classification and contouring utilizing AI

A deep learning framework, known as S-detect (S-detectTM for breast, Samsung Medison Co., Ltd., Seoul, Korea) was previously developed [25], and its performance was evaluated by this group [26]. By utilizing post-processed log-compressed data as input, the S-detect segments lesion boundaries and classifies lesions as benign or malignant.

Segmentation was performed using a modified fully convolutional network (FCN). Instead of utilizing the automatic segmentation of FCN [27], a modification was performed to receive radiologists' input for the center of a lesion, which lowers the segmentation error caused by using ultrasound images with speckle. Hence, the S-detect outputs a lesion boundary. Classification was performed using GoogLeNet [28], but after removing two auxiliary classifiers of the GoogLeNet.

The contoured lesion boundaries were used as a region of interest (ROI) for further analysis in this study, and the classification results were used to assess the performance of the DL classification.

C. Ultrasound feature extraction

To obtain more accurate classification than the DL approach, we extracted 5 ultrasound features from RF, envelope, and log-compressed data: H-scan color level, lesion boundary shape, B-mode standard deviation (STD) within the ROI, B-mode boundary STD, and Burr distribution b .

- H-scan color level: The H-scan [29], a matched filter analysis, was used to analyze the RF data and estimated frequency components of each pixel, indicating frequency shift or scatterer size. Since we utilized 256 matched filters, our analysis had 256 color levels. Lower frequency components and larger scatterers resulted in lower H-scan color levels, whereas higher frequency and smaller scatterers resulted in higher H-scan color levels. Each pixel had an estimated H-scan color level, and the estimated levels within an ROI were averaged, suggesting a parameter: the H-scan scan color level.
- Lesion boundary shape: Utilizing the lesion boundary output of the S-detect, a convex hull was calculated. The area difference (dA) between the convex hull and the lesion was measured, and dA/A was calculated for estimating the lesion boundary shape parameter where A is an area within a lesion.
- B-mode STD: Utilizing log-compressed envelope data, the STD within an ROI was calculated to characterize B-mode image texture.
- B-mode boundary STD: To investigate image texture near lesion boundaries, morphological erosion and dilation were utilized to define the inner and outer areas near the boundary, respectively. The STD within the area near the boundary was calculated. The margin length of the area is 10% of the lesion length.
- Burr distribution b : We investigated the histogram of envelope data utilizing a Burr distribution:

$$P(A) = \frac{2A(b-1)}{\lambda^2 \left[\frac{A^2}{\lambda} + 1 \right]^b} \quad (1)$$

where $P(A)$ is a probability density of an echo amplitude of A , and b is our parameter estimation, varying depending on scatterer distribution.

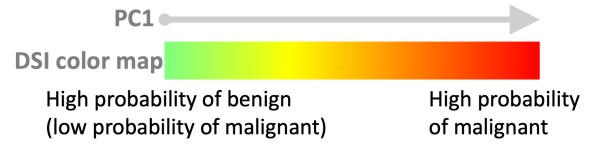


Fig. 1. A combined parameter, PC1, and corresponding DSI color map, representing probability of malignancy.

D. Multiparametric analysis and DSI

To combine the five features, a principal component analysis was performed and resulted in the first principal component (PC1) as a combined parameter. Thus, the parameter dimension of five was reduced into one while including information from all five parameters.

PC1 can correspond to a colormap as shown in Fig. 1, indicating the probability of malignancy. The combined parameter PC1 was used for visualizing breast condition within the disease-specific imaging (DSI) framework [30-32]. Each pixel in a breast lesion has a PC1 value whose corresponding DSI color level was overlaid on each pixel in a B-mode image.

III. RESULTS AND DISCUSSION

We extracted the five ultrasound features and combined them, resulting in PC1. The combined parameter PC1 is used to classify breast lesion, which can be visualized using DSI.

The performance of PC1 was compared to the DL approach (S-detect) and to radiologists. This evaluation was performed by calculating the area under the curve (AUC) for each of the three methods, as shown in Fig. 2. We divided our data into 70% of training set and 30% of testing set; AUC outputs are provided in Fig. 2 (a) and (b), respectively. To investigate performance dependence on lesion sizes, we

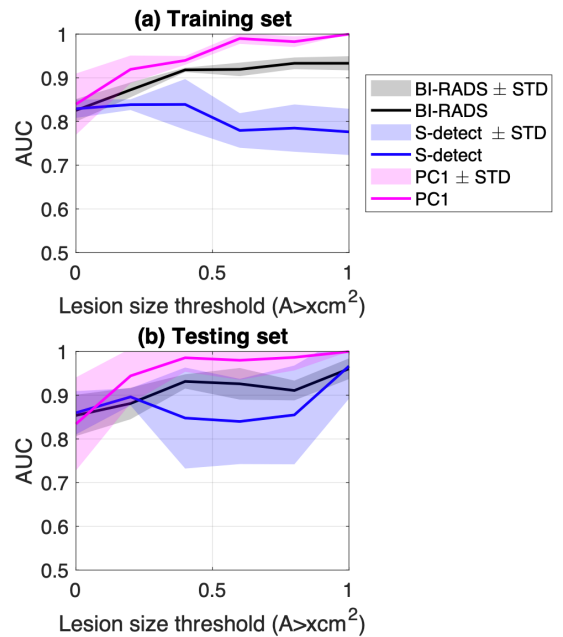


Fig. 2. Breast cancer detection results from radiologists (BI-RADS), DL (S-detect), and PC1 quantification. AUC for (a) training and (b) testing sets.

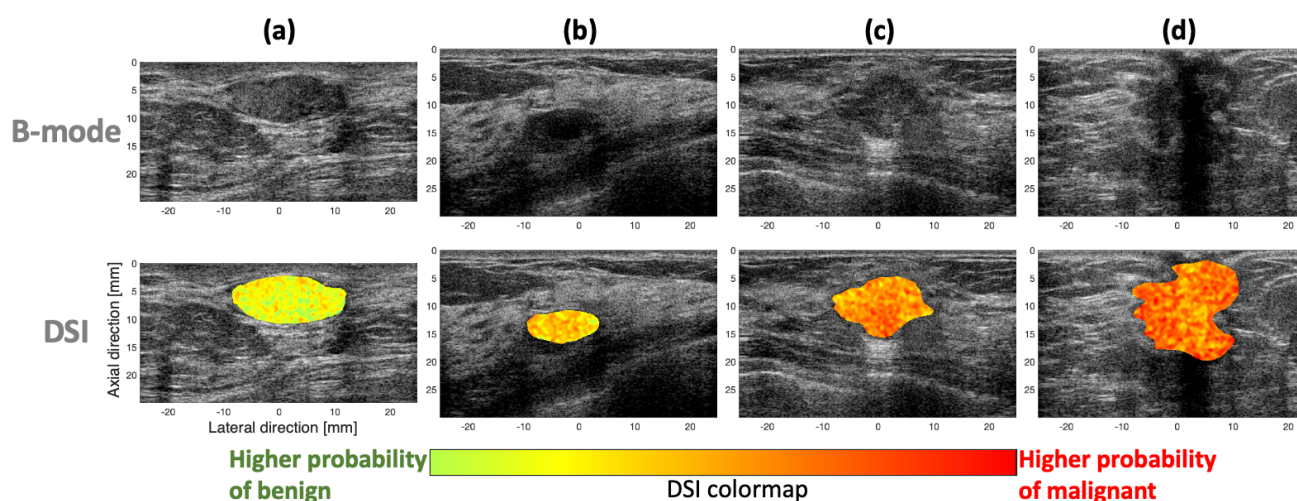


Fig. 3. DSI output. Representative images of color display overlaid on B-mode images for averaged BI-RADS scores of 3.2, 4.0, 4.5, and 5.0 from left to right. Cases (a-b) are benign, and cases (c-d) are malignant.

observed lesion size thresholds from 0 to 1 cm² in an equal interval of 0.2 cm², and thus lesions greater than a threshold were included for calculating each AUC point in Fig. 2. Fig. 2 indicates that PC1 had the highest AUC, meaning our approach outperformed radiologists and DL. Moreover, larger lesions resulted in higher AUC than smaller lesions. For the lesions greater than 0.5 cm², our PC1 achieved a high AUC greater than 0.98 for both training and testing sets.

Fig. 3 displays B-mode images and DSI results of 4 representative cases from low to high BI-RADS scores. Fig. 3 cases (a) to (d) have averaged BI-RADS scores of 3.2, 4.0, 4.5, and 5.0, which were scored by 10 radiologists and then averaged. Cases (a-b) were benign, and (c-d) were malignant. The DSI colors illustrated the probability of malignancy, showing light green to red, indicating lower to higher probability of malignancy, respectively. Thus, cases from (a) to (d) have more red pixels due to higher BI-RADS scores and higher probability of malignancy. These imaging results demonstrate that our multiparametric approach is capable of illustrating BI-RADS score differences using DSI.

IV. CONCLUSION

We proposed a breast cancer detection and visualization method, utilizing the deep learning output of breast lesion segmentation and adding more information from raw ultrasound parameters. The addition of the raw ultrasound parameters resulted in improved breast cancer diagnosis of the deep learning approach, and further, it outperformed radiologists' performance. Our approach achieved a high AUC greater than 0.98 for larger lesions (> 0.5cm²). Moreover, the DSI can visualize the probability of malignancy by providing a simple color display. Based on these results, we anticipate that the proposed analysis would assist clinicians in diagnosing breast cancer.

ACKNOWLEDGMENT

This work was supported by National Institutes of Health grant R21EB025290. The authors are grateful to colleagues who conducted this breast study and provided RF data, including Zaegyoo Hah and Yeong-Kyeong Seong at Samsung Medison.

REFERENCES

- [1] E. H. Houssein, M. M. Emam, A. A. Ali *et al.*, "Deep and machine learning techniques for medical imaging-based breast cancer: A comprehensive review," *Expert Systems with Applications*, vol. 167, pp. 114161, 2021.
- [2] N. Houssami, G. Kirkpatrick-Jones, N. Noguchi *et al.*, "Artificial Intelligence (AI) for the early detection of breast cancer: a scoping review to assess AI's potential in breast screening practice," *Expert review of medical devices*, vol. 16, no. 5, pp. 351-362, 2019.
- [3] F. Sadoughi, Z. Kazemy, F. Hamedan *et al.*, "Artificial intelligence methods for the diagnosis of breast cancer by image processing: a review," *Breast Cancer: Targets and Therapy*, vol. 10, pp. 219, 2018.
- [4] Y.-M. Lei, M. Yin, M.-H. Yu *et al.*, "Artificial intelligence in medical imaging of the breast," *Frontiers in Oncology*, pp. 2892, 2021.
- [5] L. Cai, X. Wang, Y. Wang *et al.*, "Robust phase-based texture descriptor for classification of breast ultrasound images," *Biomedical engineering online*, vol. 14, no. 1, pp. 1-21, 2015.
- [6] K. M. Prabusankaral, P. Thirumoorthy, and R. Manavalan, "Assessment of combined textural and morphological features for diagnosis of breast masses in ultrasound," *Human-centric Computing and Information Sciences*, vol. 5, no. 1, pp. 1-17, 2015.
- [7] W.-J. Wu, S.-W. Lin, and W. K. Moon, "An artificial immune system-based support vector machine approach for classifying ultrasound breast tumor images," *Journal of digital imaging*, vol. 28, no. 5, pp. 576-585, 2015.
- [8] M. Abdel-Nasser, J. Melendez, A. Moreno *et al.*, "Breast tumor classification in ultrasound images using texture analysis and super-resolution methods," *Engineering Applications of Artificial Intelligence*, vol. 59, pp. 84-92, 2017.
- [9] X. Qi, L. Zhang, Y. Chen *et al.*, "Automated diagnosis of breast ultrasonography images using deep neural networks," *Medical image analysis*, vol. 52, pp. 185-198, 2019.
- [10] Y. Xu, Y. Wang, J. Yuan *et al.*, "Medical breast ultrasound image segmentation by machine learning," *Ultrasonics*, vol. 91, pp. 1-9, 2019.
- [11] Y. Wang, E. J. Choi, Y. Choi *et al.*, "Breast cancer classification in automated breast ultrasound using multiview convolutional neural network with transfer learning," *Ultrasound in medicine & biology*, vol. 46, no. 5, pp. 1119-1132, 2020.
- [12] M. H. Yap, G. Pons, J. Martí *et al.*, "Automated breast ultrasound lesions detection using convolutional neural networks," *IEEE journal of biomedical and health informatics*, vol. 22, no. 4, pp. 1218-1226, 2017.
- [13] M. Byra, M. Galperin, H. Ojeda - Fournier *et al.*, "Breast mass classification in sonography with transfer learning using a deep convolutional neural network and color conversion," *Medical physics*, vol. 46, no. 2, pp. 746-755, 2019.

- [14] V. Kumar, J. M. Webb, A. Gregory *et al.*, "Automated and real-time segmentation of suspicious breast masses using convolutional neural network," *PloS one*, vol. 13, no. 5, pp. e0195816, 2018.
- [15] A. S. Becker, M. Mueller, E. Stoffel *et al.*, "Classification of breast cancer in ultrasound imaging using a generic deep learning analysis software: a pilot study," *The British journal of radiology*, vol. 91, no. xxxx, pp. 20170576, 2018.
- [16] J. Baek, R. Ahmed, J. Ye *et al.*, "H-Scan, Shear Wave and Bioluminescent Assessment of the Progression of Pancreatic Cancer Metastases in the Liver," *Ultrasound in Medicine and Biology*, vol. 46, no. 12, pp. 3369-3378, Dec, 2020.
- [17] J. Baek, S. S. Poul, T. A. Swanson *et al.*, "Scattering Signatures of Normal Versus Abnormal Livers with Support Vector Machine Classification," *Ultrasound in Medicine and Biology*, vol. 46, no. 12, pp. 3379-3392, Dec, 2020.
- [18] J. Baek, T. A. Swanson, T. Tuthill *et al.*, "Support vector machine (SVM) based liver classification: fibrosis, steatosis, and inflammation," *Proceedings of the 2020 Ieee International Ultrasonics Symposium (Ius)*, 2020.
- [19] J. Baek, S. S. Poul, L. Basavarajappa *et al.*, "Clusters of Ultrasound Scattering Parameters for the Classification of Steatotic and Normal Livers," *Ultrasound in Medicine & Biology*, 2021.
- [20] L. Basavarajappa, J. Baek, S. Reddy *et al.*, "Multiparametric ultrasound imaging for the assessment of normal versus steatotic livers," *Scientific reports*, vol. 11, no. 1, pp. 1-11, 2021.
- [21] J. Baek, S. S. Qin, P. A. Prieto *et al.*, "H-scan imaging and quantitative measurement to distinguish melanoma metastasis." pp. 1-4.
- [22] R. G. Gary, R. Laines, J. Pinto *et al.*, "H-scan analysis of thyroid lesions," *Journal of Medical Imaging*, vol. 5, no. 1, pp. 013505, 2018.
- [23] H. Tai, J. Song, J. Li *et al.*, "Three-dimensional H-scan ultrasound imaging of early breast cancer response to neoadjuvant therapy in a murine model," *Investigative Radiology*, vol. 57, no. 4, pp. 222-232, 2022.
- [24] W. Chen, and F. W. Samuelson, "The average receiver operating characteristic curve in multireader multicase imaging studies," *The British journal of radiology*, vol. 87, no. 1040, pp. 20140016, 2014.
- [25] S. Han, H.-K. Kang, J.-Y. Jeong *et al.*, "A deep learning framework for supporting the classification of breast lesions in ultrasound images," *Physics in Medicine & Biology*, vol. 62, no. 19, pp. 7714, 2017.
- [26] A. M. O'Connell, T. V. Bartolotta, A. Orlando *et al.*, "Diagnostic Performance of An Artificial Intelligence System in Breast Ultrasound," *J Ultrasound Med*, Mar 5, 2021.
- [27] J. Long, E. Shelhamer, and T. Darrell, "Fully convolutional networks for semantic segmentation." pp. 3431-3440.
- [28] C. Szegedy, W. Liu, Y. Jia *et al.*, "Going deeper with convolutions." pp. 1-9.
- [29] K. J. Parker, and J. Baek, "Fine-tuning the H-scan for discriminating changes in tissue scatterers," *Biomedical Physics & Engineering Express*, vol. 6, no. 4, Jul, 2020.
- [30] J. Baek, and K. J. Parker, "H-scan trajectories indicate the progression of specific diseases," *Medical Physics*, Aug 3, 2021.
- [31] J. Baek, L. Basavarajappa, K. Hoyt *et al.*, "Disease-specific imaging utilizing support vector machine classification of H-scan parameters: assessment of steatosis in a rat model," *IEEE Transactions on Ultrasonics, Ferroelectrics, and Frequency Control*, 2021.
- [32] J. Baek, and K. J. Parker, "Disease-specific imaging with H-scan trajectories and support vector machine to visualize the progression of liver diseases." pp. 1-4.